Water SA 51(3) 256–267 / Jul 2025
https://doi.org/10.17159/wsa/2025.v51.i3.4128

Research paper

Effect of the location and height of a protective spur dike on scour

Hanieh Haghighatpanah[1], Ali Hosseinzadeh Dalir[1], Payam Khosravinia[2] and Ata Amini[3]

[1]*Department of Water Engineering, Faculty of Agriculture, University of Tabriz, Tabriz, Iran*
[2]*Department of Water Sciences and Engineering, Faculty of Agriculture, University of Kurdistan, Sanandaj, Iran*
[3]*Kurdistan Agricultural and Natural Resources Research and Education Center, AREEO, Sanandaj, Iran*

Spur dikes (SD) are installed along the outer bank of a river to control river bank erosion. The first SD is more susceptible to failure due to toe scouring. A protective spur dike (PSD) is an effective measure to reduce the scouring around the nose of the first SD. In this study, experiments were conducted to determine the optimal location and height of the PSD to minimize scour depth at the nose of the first SD. The results indicate that the maximum scour depth depends on the height and distance of the PSD from the first SD. The best performance was observed when the ratio of PSD height to flow depth (H_p/y) was 1.25, and the ratio of the PSD distance from the first SD to flow depth (X_p/y) was 1.25. Scour depth at the nose of the first and second SDs was reduced by 54% and 32%, respectively. These findings suggest that PSDs can significantly reduce scour depth, thereby enhancing the effectiveness and stability of SDs.

CORRESPONDENCE
Hanieh Haghighatpanah

EMAIL
h.haghighatpanah@yahoo.com

DATES
Received: 19 February 2024
Accepted: 3 June 2025

KEYWORDS
river engineering
scour
flow separation
permeable spur dike
protective spur dike

INTRODUCTION

Scouring in river bends destroys agricultural lands and adjacent facilities. Various structures such as spur dikes (SDs), submerged spillways and submerged vanes have been proposed to control and reduce bank scouring (Abdollahpour et al., 2017; Moghadam et al., 2019). Pandey et al. (2021) investigated the influence of sediment and flow parameters on spur dike scour, for both uniform and non-uniform sediment bed surfaces. Their observations show that a decrease in sediment non-uniformity increased temporal scour depth. Tripathi and Pandey (2021) examined the local scour process around T-shaped SDs at various locations in a reverse meandering channel. Their observations showed that as the Froude number (Fr) and distance of the SD from the bend entry increased, maximum scour depth also increased. Gupta et al. (2023) studied the turbulence model and sedimentary Van Rijn model with nested mesh configuration using FLOW-3D to investigate maximum scour depth around impermeable and non-submerged spur dikes with different transverse lengths. Their observations indicated that scour depth increased with increasing spur dike length, both independently and simultaneously. Bahrami-Yarahmadi et al. (2020) experimentally studied deposition pattern and scouring around rectangular and triangular SDs. Their findings revealed that the maximum scour depth at the nose of rectangular SDs was greater than that for their triangular counterparts. Vaghefi et al. (2019) considered the length of the flow separation and reattachment zone in a 90° bend using the 'sediment simulation in intake with multiblock' (SSIIM) model. Their results showed that as the submergence ratio increased, the length of the separation and reattachment zone decreased. Yang et al. (2019) found that the main reason for the failure of SDs is the interaction of water with these structures. Abdollahpour et al. (2017) illustrated that installing SDs in river bends complicates the processes of scouring and sedimentation in this area. In sinusoidal rivers, the flow pattern in bends is highly complex and influenced by both the inner and outer banks, as well as the riverbed morphology. Over time, these factors contribute to gradual changes in the river's natural shape. Additionally, the flow pattern around SDs is affected by the formation of a series of eddies in this area (Jeon et al., 2017). Pandey et al. (2016) demonstrated that maximum shear stress occurs at the nose of SDs. Therefore, scour depth is a primary parameter in the design of SDs (Choufu et al., 2019; Nayyer, 2019). SDs are usually installed in groups, and the stability of the first SD is crucial, due to its susceptibility to failure (Pandey et al., 2016; Choufu et al., 2019).

Farshad et al. (2022) found that scour depth decreases with increasing SD permeability. The distance between SDs influences the length of the return flow, and its increase can lead to sedimentation in this area. Ezzeldin (2019), through numerical studies, investigated the effect of SD permeability on scouring, simulated with the Nays-2DH numerical model of the iRIC software package, and found that the maximum scour depth in permeable SDs was reduced by up to 68% compared to solid ones.

Nayyer et al. (2019) showed that a collar or PSD can be used to protect a group of SDs. Installing a PSD upstream of the SD group helps to divert the flow away from the first SD (Vaghefi et al., 2015). Karami et al. (2011) concluded that appropriate PSD design could significantly reduce the maximum scour depth around a group of SDs. The length of SDs has a less significant impact on the flow pattern and separation zone compared to the height and spacing of SDs (Choufu et al., 2019; Koutrouveli et al., 2019). Therefore, selecting an appropriate PSD is essential for effective river protection and management.

The stability of spur dikes (SDs) in a sinusoidal channel is significantly influenced by the presence of protective spur dikes (PSD). Despite the importance of this issue, limited research has been conducted on the effect of PSD on the stability of SDs. This study aims to experimentally investigate the optimal

location of the first SD, both with and without the implementation of PSD, to mitigate bank erosion and prevent river bank deformation. Ultimately, the results were compared with those of previous studies on changes in scour depth related to the distance between PSDs and the first SD, providing comprehensive insights into effective riverbank protection strategies. The findings of this study are expected to improve the understanding of SD stability in river bends.

MATERIALS AND METHODS

Dimensional analysis

In experimental studies of SDs, several variables influence changes in the maximum scour depth around SDs, including flow parameters, sediment properties and SD geometry. Equation 1 presents a general relationship for the dimensional analysis of the maximum scour depth (d_s) around a SD (Melville, 1992):

$$d_S = (H_P, X, X_P, X_M, L, H, L_S, W_S, \rho, \mu, V, V_C, y, g, Q, B, \alpha, \rho_S, d_{50}, A) \quad (1)$$

where: H_P is the height of the PSD, X is the distance of the first SD from the entry of the bend, X_P is the distance of the PSD from the first SD, X_M is the distance between the SDs, L is the length of the SDs, H is the height of the SDs, L_S is the length of the scour hole, W_S is the width of the scour hole, ρ is the fluid density, μ is the fluid dynamic viscosity, V is the average approaching velocity, V_C is the critical flow velocity, y is the flow depth, g is the acceleration due to gravity, Q is the flow discharge, W is the width of the channel, α is the permeability percentage, ρ_S is the density of bed particles, d_{50} is the median diameter of sediment particles, and A is the SD surface area. By applying Buckingham's π theory, the following dimensionless parameters are achieved, as shown in Eq. 2.

$$\frac{d_S}{y} = \left(\frac{H_P}{y}, \frac{X}{y}, \frac{X_P}{y}, \frac{X_M}{y}, \frac{V}{V_C}, \frac{Q}{Vy^2}, \frac{gy}{V^2}, \frac{\mu}{\rho vy}, \frac{L}{y}, \frac{B}{y}, \frac{H}{y}, \frac{L_S}{y}, \frac{W}{y}, \frac{d_{50}}{y}, \frac{A}{y^2}, \alpha\right) \quad (2)$$

The variables (L/y), (B/y), $(\rho s/\rho)$, (d_{50}/y), (A/y^2), (H/y) and α were constant in all experiments. The experiments were conducted under clear water conditions. Additionally, V/V_C and the Reynolds number were discarded in Eq. 2. Thus, the parameters investigated in this study were expressed in Eq. 3.

$$\frac{d_S}{y} = \left(\frac{H_P}{y}, \frac{X}{y}, \frac{X_P}{y}, \frac{L_S}{y}, \frac{W_S}{y}, \frac{Q}{Vy^2}\right) \quad (3)$$

Figures 1a, b and c illustrate the flow pattern and scouring mechanisms, the plan view of the SDs and the PSD and the main parameters, respectively.

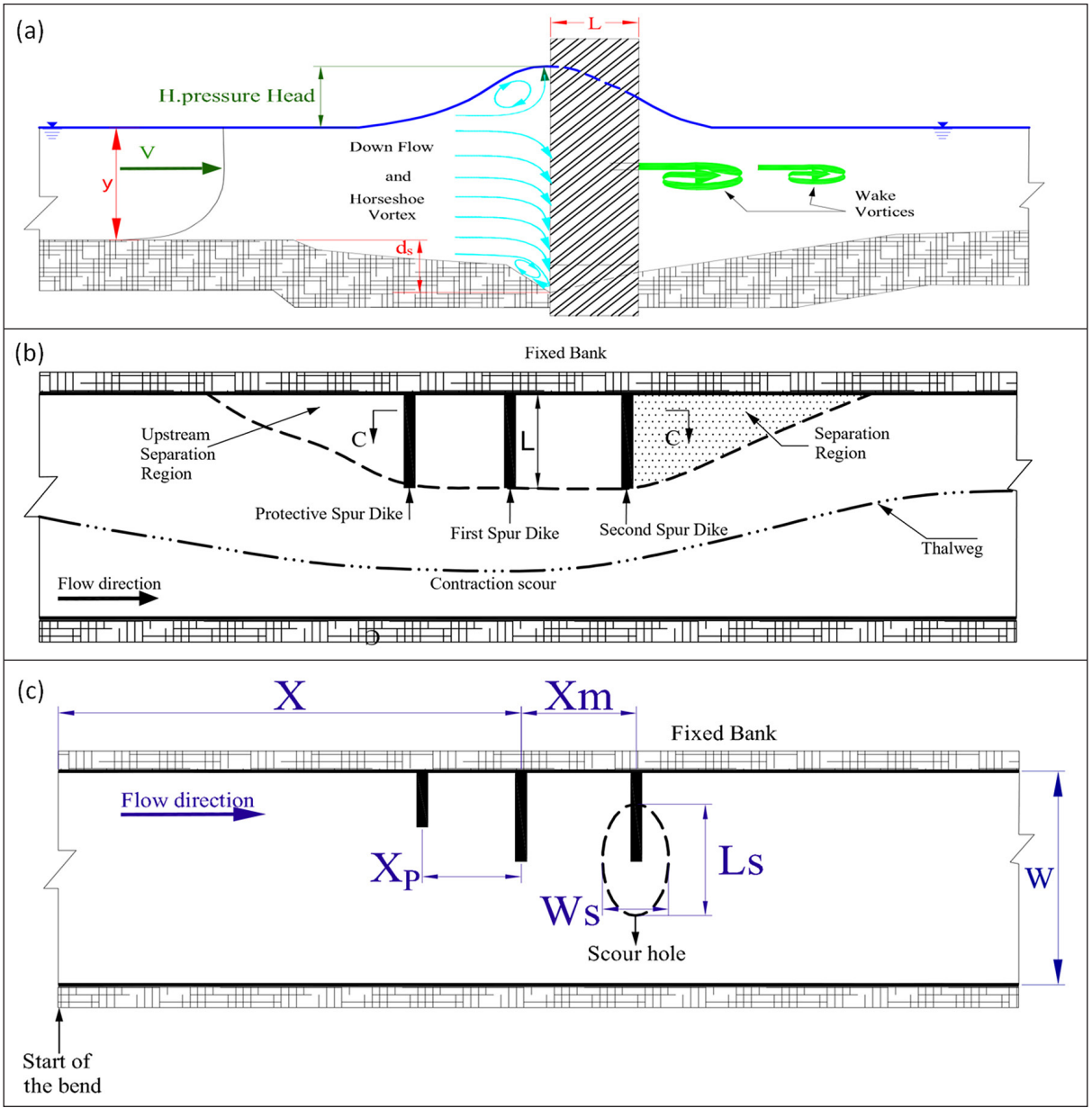

Figure 1. Flow pattern and schematic view: (a) flow pattern, (b) separation zone, and (c) parameters (adapted from Abbasi et al., 2011)

Experimental setup

The experiments were conducted in a sinusoidal channel in the hydraulic laboratory at the University of Tabriz, Iran. The flume had a rectangular cross-section with a width of 0.35 m, a height of 0.5 m, and a length of 6.7 m, with a sinusoidal coefficient of 1.12. The schematic representation (Fig. 2a) and the corresponding view of the flume and experimental setup (Fig. 2b) are presented in Fig. 2. Experiments were performed using a series of permeable SDs, consisting of two main SDs and a PSD. These structures were made from steel rods and a lattice plate, then filled to achieve 30% permeability (Fig. 2). The SDs were placed perpendicular to the flow direction in the flume. According to Choufu et al. (2019), when the SDs are positioned at 90°, a longer time period is required to reach equilibrium. In order to maintain clear water conditions during the experiments $V/V_C < 1$ (Hosseini et al., 2018; Amini et al., 2024).

Equation 4 is used to estimate the critical velocity (V_C), where U_{*C} represents the critical shear velocity. For sediment with a d_{50} < 1 mm, this critical shear velocity can be approximated using Eq. 5 (Melville, 1997).

$$\frac{V_C}{U_{*C}} = 5.75\log(5.53\frac{y}{d_{50}}) \quad (4)$$

$$U_{*C} = 0.0115 + 0.0125 d_{50}^{1.4};\ 0.1\text{mm} < d_{50} < 1\text{mm} \quad (5)$$

According to the mentioned equations, the values of V/V_C were maintained within the range of 0.65 to 0.83 to ensure clear water conditions in the flume. The flow depth in the laboratory channel was kept to 16 cm using an adjustable tailgate at the end of the channel (Fig. 2). The sediments used in the experiments were nearly uniform, with d_{50} = 0.9 mm, and a standard deviation σ_g = 1.35 (Amini and Solaimani, 2018; Coleman et al., 2003), coefficient of uniformity C_u = 1.96, coefficient of curvature C_c = 0.92 and a thickness of 10 cm in the laboratory flume.

In experiments investigating scour around hydraulic structures, the width of the flume and the model scale can significantly influence local scour due to the contraction scour effect (Ahmed et al., 2021). Brown et al. (1985) recommended that the length of the SDs should be less than 15% of the channel width to prevent cross-section contraction. Based on this recommendation, the SD length (L) in this study was set to 5 cm for all SDs. Brown et al. (1985) concluded that the distance between the SDs should be 2 to 6 times their length to provide better riverbank protection. Therefore, in this study, X_M, was set as 3L. The water level during the experiments was measured using an ultrasonic distance sensor (Data logic, model US30) with an accuracy of ±0.1 mm. Discharge and bed topography were recorded at the end of the experiments, after draining the channel, using an ultrasonic flow meter (model TDS-100) with an accuracy of ±0.1 L/s and a laser distance meter (model SW-S70), with an accuracy of ±0.1 mm, respectively. At the beginning of the channel, two flow-calming sections were installed: a baffle wall as the first section and brick as the second. Additionally, a baffle weir was placed at the end of the channel to stabilize the flow and dissipate eddies (Fig. 2a).

Experiments

In this study, three series of experiments were conducted. To investigate the effect of the PSD in reducing scour around the SDs, the first and second series of experiments were performed with and without a PSD, along the length of the bend to determine the optimal location of the first SD. Figure 3 illustrates the locations of the first SD along the bend for both the first and second series of experiments, along with the corresponding values of X. These locations are labelled from A through J.

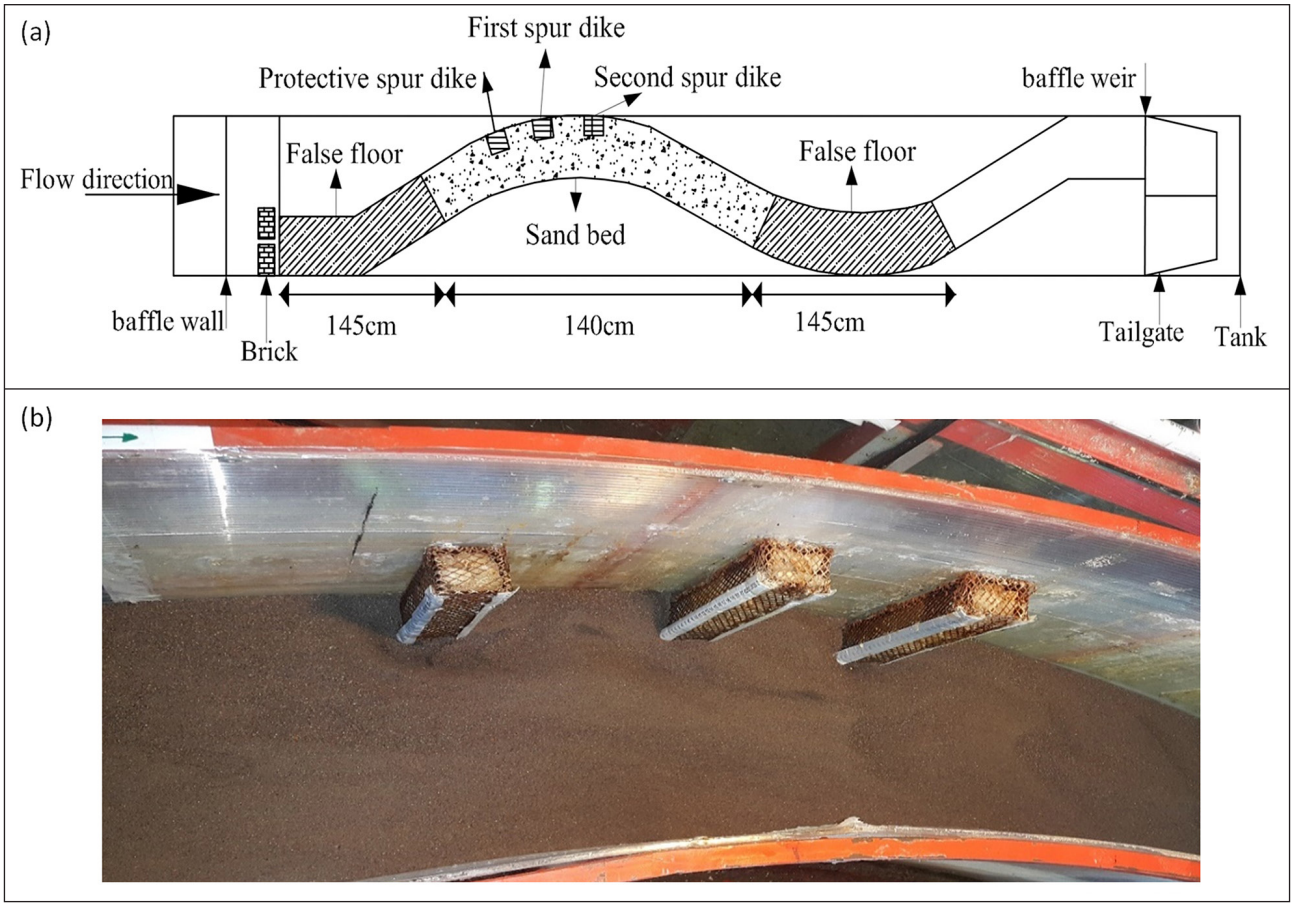

Figure 2. Schematic view of experimental setup: (a) a schematic of the flume, (b) a view of the test area

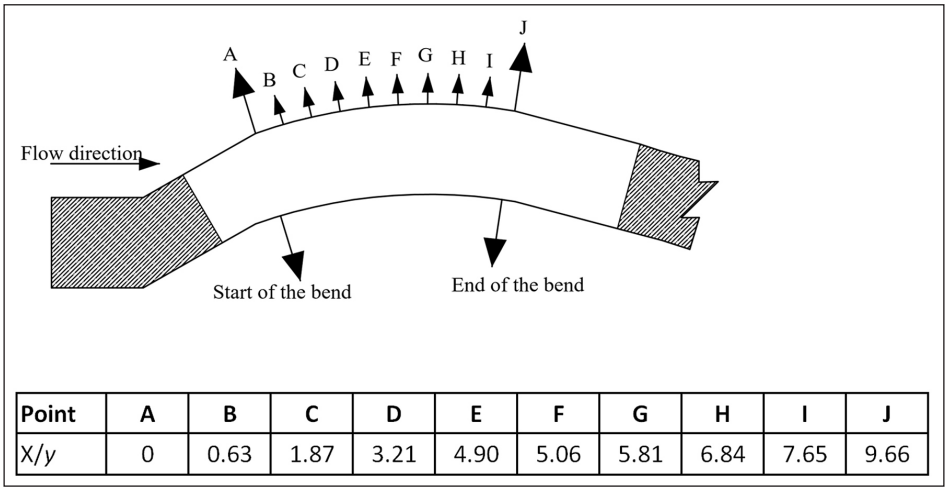

Point	A	B	C	D	E	F	G	H	I	J
X/*y*	0	0.63	1.87	3.21	4.90	5.06	5.81	6.84	7.65	9.66

Figure 3. The location of the SDs with respect to the entry of the bend

Table 1. Parameters investigated in the present study

Exp. run	Q (L/s)	Fr	Re	Re*	X_P	H_P	Exp. run	Q (L/s)	Fr	Re	Re*	X_P	H_P
1	14	0.2	20 750	71.4	2L	0.14	19	14	0.2	20 750	71.4	2L	0.18
2			23 714		3L		20			23 714		3L	
3			26 679		4L		21			26 679		4L	
4	16	0.23	20 750	71.4	2L	0.14	22	16	0.23	20 750	71.4	2L	0.18
5			23 714		3L		23			23 714		3L	
6			26 679		4L		24			26 679		4L	
7	18	0.26	20 750	71.4	2L	0.14	25	18	0.26	20 750	71.4	2L	0.18
8			23 714		3L		26			23 714		3L	
9			23 714		4L		27			23 714		4L	
10	14	0.2	20 750	71.4	2L	0.16	28	14	0.2	20 750	71.4	2L	0.2
11			23 714		3L		29			23 714		3L	
12			26 679		4L		30			26 679		4L	
13	16	0.23	20 750	71.4	2L	0.16	31	14	0.23	20 750	71.4	2L	0.2
14			23 714		3L		32			23 714		3L	
15			26 679		4L		33			26 679		4L	
16	18	0.26	20 750	71.4	2L	0.16	34	14	0.26	20 750	71.4	2L	0.2
17			23 714		3L		35			23 714		3L	
18			26 679		4L		36			26 679		4L	

In the third series of experiments, the first SD was positioned at a location in the bend where the flow pattern changed, increasing the possibility of deformation. The PSD was placed upstream of the first SD at 3 distances: X_p/y= 0.63, 0.94 and 1.25. To investigate both submerged and non-submerged conditions, 4 PSD heights were considered: H_p/y =1.25, 1.13, 1 and 0.88. All experiments were conducted under subcritical flow regime with different Froude numbers (Fr). The values of the parameters examined in this study are presented in Table 1 (Re = Reynolds number, Re* = shear Reynolds number).

RESULTS AND DISCUSSION

Scour formation

The SDs significantly influence the flow dynamics within the flume, primarily by reducing the cross-sectional area. Variations in flow patterns were observed at the tips of the spur dikes, attributed to differences in geometric and other relevant technical specifications. After the flow was regulated and stabilized within the channel, an increase in velocity and shear stress was observed in the bends. This increase, resulting from the constriction of the cross-sectional area, gradually initiated scouring and erosion around the spur dikes. Scouring at the nose of the first SD began with greater velocity and intensity compared to the second SD. Additionally, scouring at the nose of the second SD occurred with a slight time delay of a few seconds. Observations indicated that, after colliding with the first SD, the flow was deflected toward the centre of the channel, gradually reducing its intensity at the nose of the second SD. When the PSD was placed upstream of the first SD, the location of maximum shear stress was shifted to the nose of the PSD. As a result, the maximum scour depth at the SDs was reduced due to the decreased flow intensity upstream of the first SD.

Equilibrium scouring time

In order to achieve maximum scour depth (d_{se}), the test duration (t_e) was set to 391 min; t_e is (time to equilibrium) is defined as the

point at which 90% of the maximum scour depth has developed. Beyond this time, further changes in scour depth are minimal (Melville and Chiew, 1999). After t_e, only slight changes in scour depth occurred. The development of scour over time and its comparison with previous studies are presented in Fig. 4.

Location of first spur dike

In the first series of experiments, the ratio X/y was varied from 0 to 9.66 along the bend. The least scour depth was observed when the first SD was placed at the entry of the bend, corresponding to $X/y = 1.87$ (Points A to C in Fig. 3).

Beyond Point C, the scour depth increased as the SDs were relocated further along the bend, reaching its peak near the apex of the bend at Point E. The maximum scour depth was observed at the nose of the bend, identified as Point I. This scouring phenomenon can be attributed to the centrifugal forces generated as the flow moves through the bend (Vaghefi et al., 2015). These forces create a cross-flow within the bend, which, when combined with the longitudinal flow, from a spiral flow. This spiral flow becomes fully developed as it progresses along the bend and nears the apex. The placement of SDs within the flow path intensified this process by concentrating velocity at the nose of the SDs, leading to an increase in both the depth and dimensions of the scour hole. As the distance from the bend entry increased and the SDs approached the apex, the scouring effect become more pronounced. Due to the curvature of the bend, the flow deviated into the embayment zone, increasing the length of the flow separation region (Tripathi and Pandey, 2021). Figure 5 compares the results of this study with those reported by Tripathi and Pandey (2021).

Protective spur dike

In the second series of experiments, a PSD was used in conjunction with the main SDs. The results from the initial series served as control experiments, enabling the assessment of the PSDs impact on reducing scour depth. Table 2 presents the variations in the maximum scour depth (d_s), length (L_s) and width (W_s) of the scour hole for the main SDs at Points A to J, both with and without a PSD.

The interaction between the flow and SDs led to the formation of downflow upstream of the SDs, which acted as the primary factor in local scouring. This downflow lifted sediments around the SDs and transported them downstream. Additionally, a horseshoe vortex formed due to the separation of streamlines caused by the presence of the SDs in the flow path. Although the power and size of this vortex were weak at the beginning of the experiment, they intensified as the scour hole developed around the SDs. These eddies further contributed to the expansion of the scour hole downstream of the SDs. The scour depth at the nose of the first SD increased due to the influence of secondary flow in this region (Vaghefi et al., 2019). Over time, the depth and width of the scour holes at the SD's noses expanded. The scouring rate was initially high; however, as the scour hole grew, the intensity of the downflow gradually decreased. Eventually, the scour depth reached equilibrium.

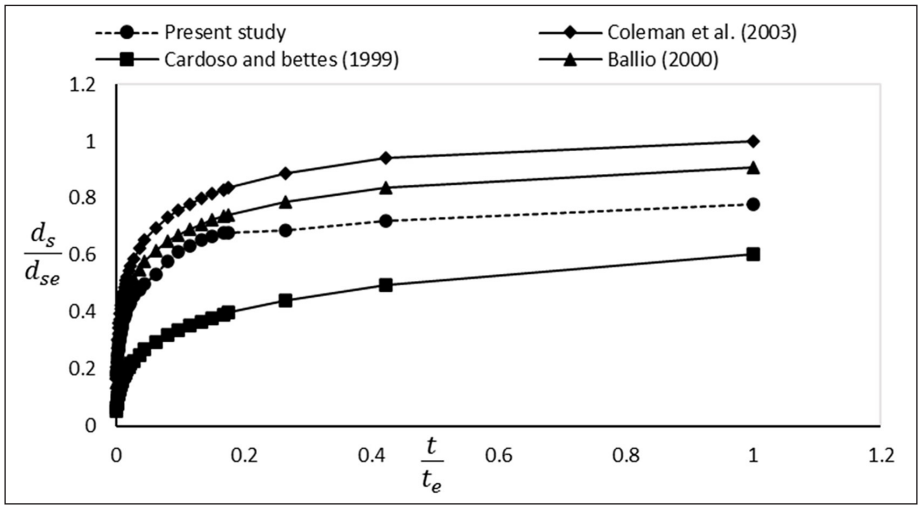

Figure 4. Scour depth variation in terms of time in the vicinity of first SD

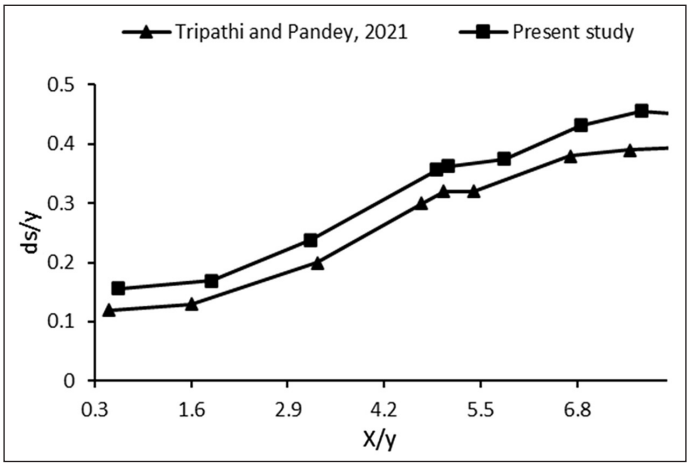

Figure 5. Comparison of this study with Tripathi and Pandey (2021)

Table 2. Changes in the depth, length, and width of the scour hole around the main SDs, with and without PSD

X	d_S/y	d_{SP}/y	Reduction %	L_S/y	L_{SP}/y	Reduction %	W_S/y	W_{SP}/y	Reduction %
					First SD				
A	0.14	0.04	72.7	0.25	0.13	50.0	0.66	0.13	81.0
B	0.16	0.04	76.0	0.38	0.13	66.7	0.81	0.13	84.6
C	0.17	0.04	74.1	0.38	0.34	8.3	0.75	0.56	25.0
D	0.24	0.05	78.9	0.59	0.38	36.8	0.84	0.69	18.5
E	0.36	0.06	84.2	0.59	0.47	21.1	1	0.72	28.1
F	0.36	0.06	82.8	0.56	0.47	16.7	1.06	0.69	35.3
G	0.38	0.08	80.0	0.63	0.41	35.0	1.13	0.63	44.4
H	0.43	0.08	82.6	0.66	0.31	52.4	1.13	0.69	38.9
I	0.46	0.11	76.7	0.69	0.31	54.5	1.19	0.69	42.1
J	0.44	0.06	85.7	0.63	0.19	70.0	1.22	0.31	74.4
					Second SD				
A	0.13	0.06	50.0	0.18	0.13	28.6	0.44	0.41	7.1
B	0.13	0.09	25.0	0.19	0.13	33.3	0.5	0.5	0.0
C	0.16	0.09	42.3	0.41	0.22	46.2	0.75	0.44	41.7
D	0.18	0.10	42.9	0.34	0.25	27.3	0.88	0.59	32.1
E	0.18	0.16	13.8	0.34	0.31	9.1	0.94	0.69	26.7
F	0.21	0.21	2.9	0.38	0.34	8.3	0.75	0.69	8.3
G	0.28	0.22	20.5	0.38	0.31	16.7	0.75	0.63	16.7
H	0.31	0.23	28.0	0.38	0.28	25.0	1.06	0.66	38.2
I	0.33	0.23	30.2	0.22	0.19	14.3	1.06	0.63	41.2
J	0.25	0.19	25.0	0.28	0.25	11.1	1.13	0.63	44.4

Lifted particles were gradually transported from the nose of the first SD into the scouring hole around the second SD. However, these sediments were displaced by horseshoe vortices, leading to the formation of downflow around the second SD in a similar manner. The lifted particles were carried from the front of the SDs to the downstream section of the channel, resulting in the formation of ripples. Due to the pressure differentials, vortices developed behind these ripples, causing them to be transported further downstream within the channel.

Index P (Table 2) is related to the condition where the main SDs were placed along the bend with a PSD.

Table 2 presents statistical information on the inputs for this series of experiments, showing that $0.14 < d_S/y < 0.44$, $0.25 < L_S/y < 0.63$ and $0.66 < W_S/y < 1.22$. According to Table 2, the maximum scour depth at the nose of the SDs increased as the location of the SDs approached the apex of the bend, both with and without the presence of a PSD. However, when the PSD was placed upstream of the first SD, a significant reduction in maximum scour depth was observed. This indicates that the effectiveness of the PSD improves as the distance between the first SD and the entrance of the bend increases. The reductions in scour depth at the nose of the first SD with the inclusion of a PSD at Points D, E, F, G, H, and I were 78%, 84%, 82%, 80%, 82%, and 76%, respectively. Table 2 also shows that both the length and width of the scour hole increased along the bend, regardless of the presence of a PSD. However, when the PSD was positioned upstream of the first SD, these values were notably reduced. Additionally, there was a significant decrease in both the dimensions of the scour hole and the volume of sediment particles displaced from the nose of the main SDs. With the presence of a PSD, the maximum scour depth and scour hole dimensions around the second SD were lower than those around the first SD. This occurred because the first SD acted as a PSD for the second SD. Based on these values, the PSD further reduced the depth and dimensions of the scour hole around the second SD. When the first SD was placed at Point J, the scour depth at the nose of the first and second SDs was reduced by approximately 85% and 25%, respectively, in the presence of the PSD. Additionally, the length of the scour hole around the first and second SDs decreased by 70% and 11%, respectively. Similarly, the width of the scour hole around the main SDs at this point was reduced by approximately 74% and 44%, respectively (Table 2).

Figure 6 illustrates the reduction in maximum scour depth around the main SDs when a PSD is present at $X/y = 1.87$. According to the diagrams in this figure, when the main SDs were placed along the bend without a PSD, there was a continuous increase in scouring at the nose of the main SDs, and the scour depth increased rapidly. However, when a PSD was positioned upstream of the main SDs, the scour depth at their nose increased only during the initial minutes of the experiment (Fig. 6, Zone A and C) after which it decreased significantly (Fig. 6, Zones B and D).

The PSD reduced the intensity of the downflow and horseshoe vortex by diverting flow away from the nose of the main SDs, particularly the first one. This flow diversion led to the formation of a secondary scour hole near the nose of the first SD. As this hole developed, lifted particles were transferred from it to the scour holes around the main SDs. Initially, sediment particles were carried from the nose of the PSD and the secondary hole to the scour hole around the first SD (Fig. 6a). As a result, the scour depth at the nose of the first SD temporarily decreased to zero (Zone B in Fig. 6a). Over time, the scour depth at the nose of the first spur dike (SD) gradually increased and reached equilibrium after 391 min. The scour depth at the nose of the second SD initially increased (Zone C, Fig. 6b). This was due to sediments being transported from the nose of the first SD and subsequently settling in the scour hole around the second SD. However, after

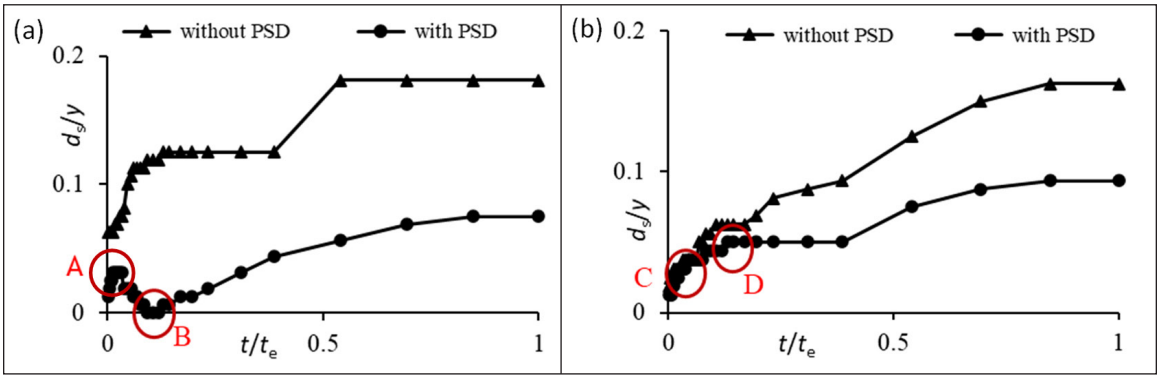

Figure 6. Reduction of maximum scour depth around SDs with the presence of PSD: (a) first SD and (b) second SD

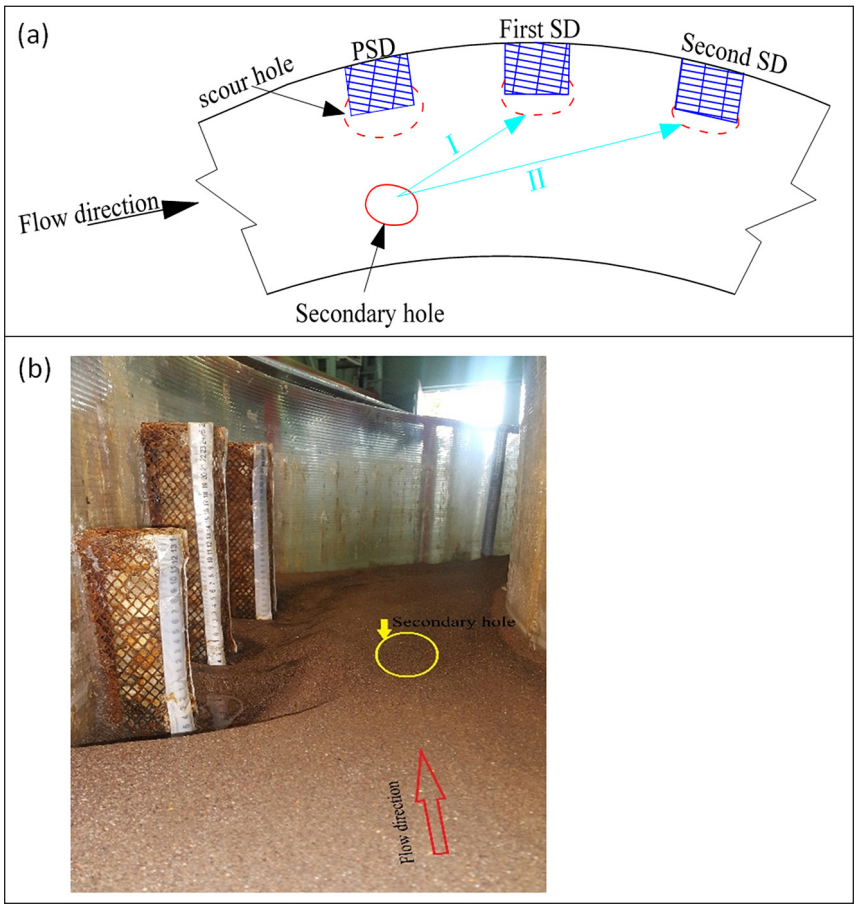

Figure 7. (a) Formation of the secondary hole, and (b) transformation of lifted particles to the scour hole which was formed around SDs where H_p/y = 1.25, X_p = 3L and Fr = 0.26

a certain period, the scour depth at the nose of the second SD stabilized and remained unchanged (Zone D in Fig. 6b). This stabilization coincided with the formation of downflows in this region, which quickly flushed out accumulated sediments from the scour hole. Following this stabilization period, the scour depth at the nose of the second SD experienced a slight increase before reaching equilibrium. The formation and location of the secondary hole in the flume are shown in Fig. 7.

Optimizing the height and location of the protective spur dike

In the third series of experiments, based on the results of previous experiments, the first SD was installed at X/y = 1.87. To assess the impact of H_p and X_p on the scour depth at the nose of the main SDs, a PSD with varying H_p and X_p values was placed upstream of main SDs.

Height

Four different PSD heights were considered: H_p/y = 1.25, 1.13, 1 and 0.88. For each height, experiments were conducted at 3 Froude numbers and for 3 distances between the PSD and the main SD, corresponding to X_p = 4L, 3L and 2L as illustrated in Fig. 8.

The data presented in the graphs indicate that the maximum scour depth (d_s) occurred at an H_p/y ratio of 0.88. As the H_p/y ratio increased to 1.0, the maximum scour depth at the first SD showed a slight decrease, at approximately 22% lower than the maximum value observed at H_p/y = 0.88 (Fig. 8e). Furthermore, when the H_p/y ratio increased to 1.13, the scour depth at the first SD was 7% lower than the maximum value recorded at the optimal H_p/y ratio of 0.88. Notably, as the H_p/y ratio increased to its highest value of 1.25, the scour depth at the first SD decreased significantly

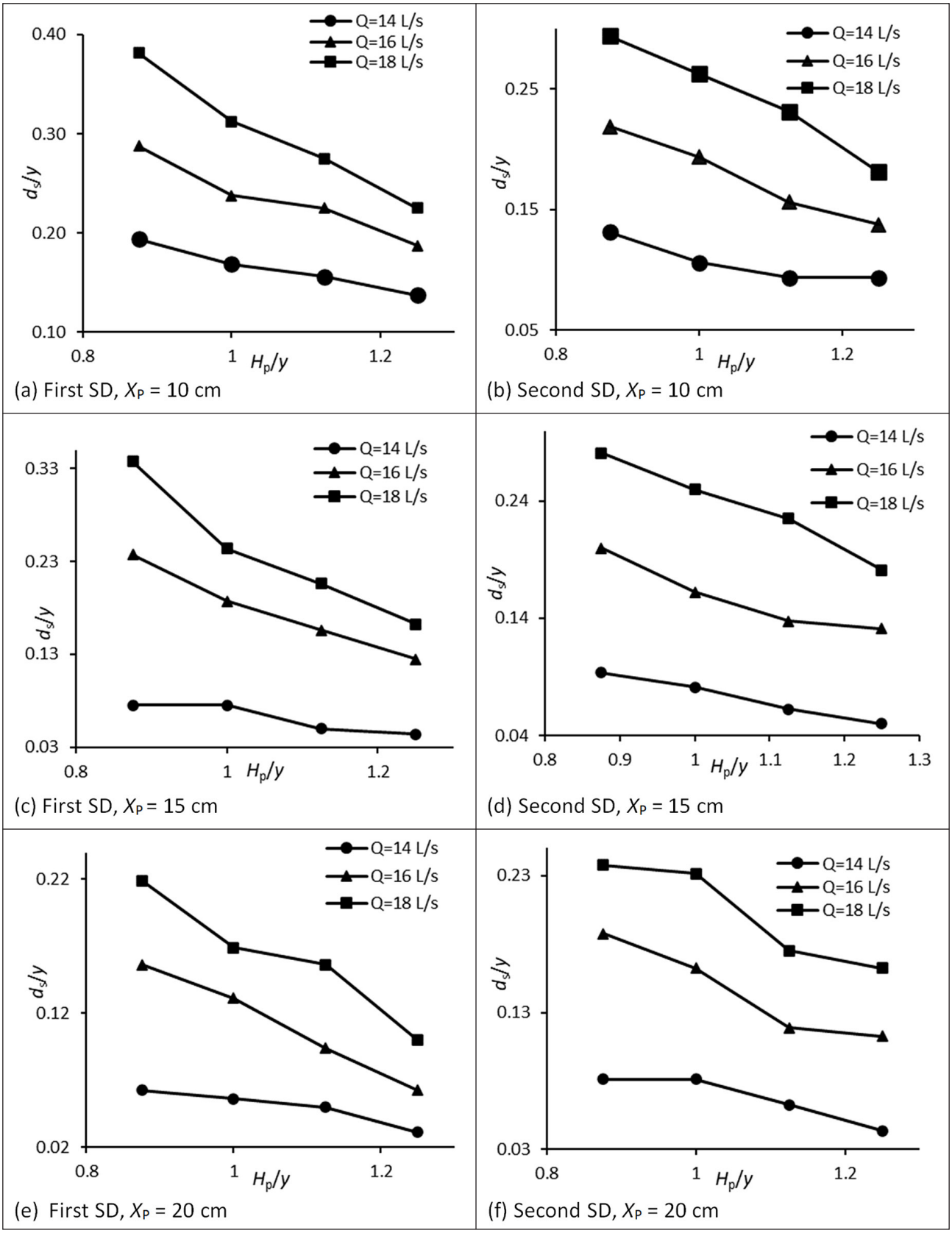

Figure 8. The effect of height of PSD on reduction of scour depth at the nose of the main SDs at various distance

compared to the three lower H_p/y ratios, as illustrated in Fig. 8e. Observations indicated that at H_p/y = 0.88, the formation and development of the secondary hole progressed slowly and did not advance significantly compared to the other height ratios. This suggests that the submerged PSD had a limited effect on deflecting flow away from the nose of the main SDs. Since the flow passed over both the top and front of the submerged PSD, it reached the nose of the first SD with greater power and intensity, leading to increased scour around the main SDs. In contrast, The PSD with H_p/y = 1.25 facilitated the formation and development of a secondary hole more rapidly than the other height ratios. The emergence of this hole in the initial minutes of the experiments indicated an effective diversion of flow, which reduced both the power and intensity of the flow around the main SDs.

Table 3. The rate of scour depth reduction at the nose of the main SDs at different distances and heights of the PSD

X_P	Q (L/s)	$H_P/y = 0.88$	$H_P/y = 1$	$H_P/y = 1.13$	$H_P/y = 1.25$	Reduction %
		d_S/y	d_S/y	d_S/y	d_S/y	H_P = 14 vs. 20 cm
				First SD		
2L	14	0.19	0.17	0.16	0.14	29.0
	16	0.29	0.24	0.23	0.19	34.8
	18	0.38	0.31	0.28	0.23	41.0
3L	14	0.08	0.08	0.05	0.04	41.7
	16	0.24	0.19	0.16	0.13	47.4
	18	0.34	0.24	0.21	0.16	51.9
4L	14	0.06	0.06	0.05	0.03	50.0
	16	0.16	0.13	0.09	0.06	60.0
	18	0.22	0.17	0.16	0.10	54.3
				Second SD		
2L	14	0.13	0.11	0.09	0.09	28.6
	16	0.22	0.19	0.16	0.14	37.1
	18	0.29	0.26	0.23	0.18	38.3
3L	14	0.09	0.08	0.06	0.05	46.7
	16	0.20	0.16	0.14	0.13	34.4
	18	0.28	0.25	0.23	0.18	35.6
4L	14	0.08	0.08	0.06	0.04	46.2
	16	0.19	0.16	0.12	0.11	40.0
	18	0.24	0.23	0.18	0.16	31.6

During the initial minutes of the experiments, the transport of lifted particles from the secondary hole to the scour hole around the main SDs prevented any increase in scour depth around the main SDs. However, as time progressed and the system approached equilibrium, the development of the secondary hole slowed significantly and nearly ceased due to a reduction in flow velocity and downward forces in the area between the submerged PSD and the main SDs. This decrease in maximum scour depth was accompanied by sedimentation in this region, consistent with the findings of Karami et al. (2011). According to Table 3, scour depth (d_S) increased with higher Froude numbers, aligning with the observations of Masjedi et al. (2010) and Vaghefi et al. (2015). Additionally, as the height of the PSD increased, the width of the shear layer and the dimensions of the scour hole around the main SDs decreased. The dimensionless values of scour depth at the nose of the main SDs (d_S/y) are presented in Table 3.

Table 3 shows that the presence of the PSD prevented a significant increase in scour with increasing flow discharge. The maximum reduction in scour depth at the nose of the main SDs was observed at H_P/y = 1.25 and X_P = 4L. As indicated in Table. 3, increasing H_P/y from 0.88 to 1.25 resulted in a maximum scour depth reduction of 50% at the nose of the first SD and 46% at the nose of the second SD. Additionally, the scour depth at the nose of the second SD was lower than at the first SD.

Distance

One of the key parameters in the design of the PSD is its distance from the first SD (Vaghefi et al., 2015). In this study, 3 distances (X_P = 2L, 3L and 4L) were investigated at 4 heights (H_P/y = 1.25, 1.13, 1, and 0.88) across 3 Froude numbers (Fr = 0.2, 0.23, and 0.26). The relationship between these variables is illustrated in Fig. 9.

Figure 9 illustrates the effect of different X_P/y values on d_S/y for various PSD heights. As X_P increased, the maximum scour depth around the main SDs decreased. The highest scour depth was recorded at X_P = 2L and Fr = 0.26. As shown in Fig. 9g, increasing X_P to 3L significantly reduced the scour depth by approximately 68%. Further increasing X_P from 3L to 4L resulted in an additional 28% reduction in scour depth.

The length of the flow separation zone is influenced by X_P and increases as X_P expanded. At X_P = 2L, there was insufficient space for the transfer of lifted particles from the nose of the PSD and the secondary hole to the scour hole around the main SDs, particularly the first one. as a result, sediments bypassed the first SD's scour hole. With an increase in X_P, the length of the return flow also grew, leading to the formation of a low-velocity zone around the SDs, which facilitated sedimentation between them. This observation aligns with the findings of Karami et al. (2011) and Vaghefi et al. (2015). Two opposite vortices formed between the first SD and the PSD. The counter-clockwise vortex had a destabilizing effect on the stability of the channel, increasing the size of the flow separation zone and threatening channel stability (Vaghefi et al., 2015).

Within the region of the PSD, bed shear stress increased, while shear stress on the channel walls decreased, leading to the formation of a complete vortex at X_P = 4L. This vortex facilitated scouring and sediment transport to the scour holes around the main SDs. However, this study found that increasing X_P beyond 4L did not further enhance the stability of the main SDs. In Fig. 10, the results of this study are compared with those of Karami et al. (2011).

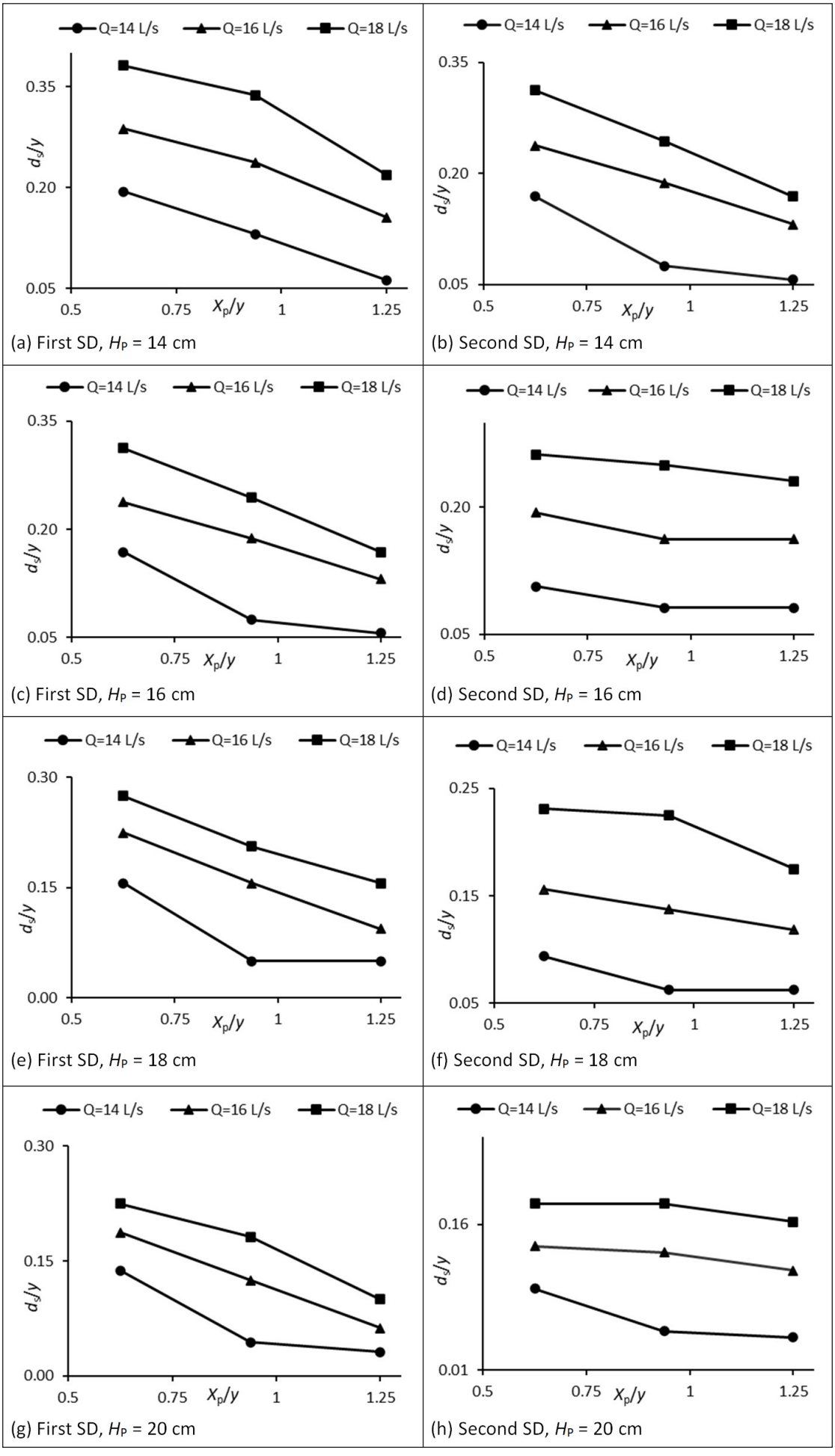

(a) First SD, H_P = 14 cm
(b) Second SD, H_P = 14 cm
(c) First SD, H_P = 16 cm
(d) Second SD, H_P = 16 cm
(e) First SD, H_P = 18 cm
(f) Second SD, H_P = 18 cm
(g) First SD, H_P = 20 cm
(h) Second SD, H_P = 20 cm

Figure 9. The effect of distance of PSD on reduction of the scour depth at the nose of the main SDs

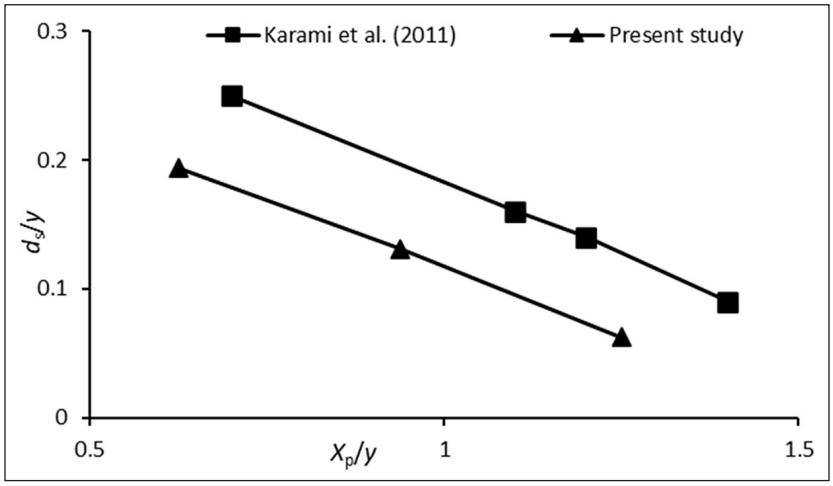

Figure 10. Comparison of the results of this study with that of Karami et al. (2011)

CONCLUSION

In the present study, an initial set of 20 experiments was conducted to determine the optimal positioning of the first spur dike (SD) at various distances from the bend entry. These experiments were divided into two series: one with a protective spur dike (PSD) and the other without it. Following this, a third series of 36 experiments was performed to investigate the effects of different PSD heights and distances under various Froude numbers, with the goal of minimizing scour around the main SD located at the channel bend. The main findings of this research are as follows:

- The PSD led to the formation of a secondary hole near the scour hole of the first SD, significantly reducing the maximum scour depth around the main SDs.
- The height of the PSD had a substantial impact on flow deflection away from the nose of the main SDs. The best performance in reducing scour depth was observed within the range of $1.13 \leq H_p/y \leq 1.25$.
- Increasing the distance between the PSD and the first SD improved streambed stability by extending the flow separation zone. This finding suggests that a slight reduction in scour depth is associated with the range of $3 \leq X_p/L \leq 4$.

ORCIDS

Hanieh Haghighatpanah
https://orcid.org/0000-0003-2812-5916

Ali Hosseinzadeh Dalir
https://orcid.org/0000-0003-2359-3921

Payam Khosravinia
https://orcid.org/0000-0002-8524-6469

Ata Amini
http://orcid.org/0000-0001-9358-185X

REFERENCES

ABBASI S, KAMANBEDAST A and AHADIAN J (2011) Numerical investigation of angle and geometric of l-shape groin on the flow and erosion regime at river bends. *World Appl. Sci. J.* **15** (2) 279–284.

ABDOLLAHPOUR M, HOSSEINZADEH DALIR A, FARSADIZADEH D and GUALTIERI C (2017) Experimental study on erosion and sedimentation patterns downstream of a W-weir in a sinusoidal mild bend. *Water* **9** (9) 638. https://doi.org/10.3390/w9090638

AHMED O, AMINI A, BAHRAMI J, KAVIANPOUR MR and HAWEZ DM (2021) Numerical modeling of depth and location of scour at culvert outlets under unsteady flow conditions. *J. Pipeline Syst. Eng. Pract.* **12** (41) Article 04021040. https://doi.org/10.1061/(ASCE)PS.1949-1204.0000578

AMINI A and SOLAIMANI N (2018) The effects of uniform and nonuniform pile spacing variations on local scour at pile groups. *Mar. Georesour. Geotechnol.* **36** (7) 861–866. https://doi.org/10.1080/1064119X.2017.1392658

AMINI A, MAHMMOD T and GHAZALI A (2024) Optimizing and evaluation of scour depth prediction techniques for columns as a component of complex bridge piers. *Adv. Civ. Eng. and Environmental Science* 1 (1) 64–69. https://doi.org/10.22034/acees.2024.477822.1008

BALLIO F and ORSI E (2001) Time evolution of scour around bridge abutments. *Water Eng. Res.* **2** (4) 243–259.

BAHRAMI-YARAHMADI M, PAGLIARA S, YABAREHPOUR E and NAJAFI N (2020) Study of scour and flow patterns around triangular-shaped spur dikes. *KSCE J. Civ. Eng.* **24** (11) 3279–3288. https://doi.org/10.1007/s12205-020-2261-x

BROWN MJ (1985) Effect of grain straw and furrow irrigation stream size on soil erosion and infiltration. *J. Soil Water Conserv.* **40** (4) 389–391. https://doi.org/10.1080/00224561.1985.12435699

CARDOSO AH and BETTESS R (1999) Effects of time and channel geometry on scour at bridge abutments. *J. Hydraul. Eng.* **125** (4) 388–399. https://doi.org/10.1061/(ASCE)0733-9429(1999)125:4(388)

CHOUFU L, ABBASI S, POURSHAHBAZ H, TAGHVAEI P and TFWALA S (2019) Investigation of flow, erosion, and sedimentation pattern around varied groynes under different hydraulic and geometric conditions: a numerical study. *Water* **11** (2) 235. https://doi.org/10.3390/w11020235

COLEMAN SE, LAUCHLAN CS and MELVILLE BW (2003) Clear-water scour development at bridge abutments. *J. Hydraul. Res.* **41** (5) 521–531. https://doi.org/10.1080/00221680309499997

EZZELDIN RM (2019) Numerical and experimental investigation for the effect of permeability of spur dikes on local scour. *J. Hydroinf.* 21 (2) 335–342. https://doi.org/10.2166/hydro.2019.114

FARSHAD R, KASHEFIPOUR SM, GHOMESHI M and OLIVETO G (2022) Temporal scour variations at permeable and angled spur dikes under steady and unsteady flows. *Water* **14** (20) 3310. https://doi.org/10.3390/w14203310

GUPTA LK, PANDEY M and RAJ PA (2023) Numerical modeling of scour and erosion processes around spur dike. *Clean Soil, Air, Water* 2300135. https://doi.org/10.1016/j.ijsrc.2020.03.015

JEON OH, KIM C, LABERGE RM, DEMARIA M, RATHOD S, VASSEROT AP and ELISSEEFF JH (2017) Local clearance of senescent cells attenuates the development of post-traumatic osteoarthritis and creates a pro-regenerative environment. *Nat. Med.* **23** (6) 775–781. https://doi.org/10.1038/nm.4324

KARAMI MOGHADAM M, AMINI A, MALEK MA, MOHAMMAD T and HOSEINI H (2019) Physical modeling of ski-jump spillway to evaluate dynamic pressure. *Water* **11** (8) 1687. https://doi.org/10.3390/w11081687

KARAMI H, ARDESHIR A, BEHZADIAN K and GHODSIAN M (2011) Protective spur dike for scour mitigation of existing spur dikes. *J. Hydraul. Res.* **49** (6) 809–813. https://doi.org/10.1080/00221686.2011.625166

KOUTROUVELI TI, DIMAS AA, FOURNIOTIS NT and DEMETRACOPOULOS AC (2019) Groyne spacing role on the effective control of wall shear stress in open-channel flow. *J. Hydraul. Res.* **57** (2) 167–182. https://doi.org/10.1080/00221686.2018.1478895

MASJEDI A, BEJESTAN MS and ESFANDI A (2010) Experimental study on local scour around single oblong pier fitted with a collar in a 180-degree flume bend. *Int. J. Sedim. Res.* **25** (3) 304–312. https://doi.org/10.1016/S1001-6279(10)60047-9

MELVILLE BW (1992) Local scour at bridge abutments. *J. Hydraul. Eng.* **118** (4) 615–631. https://doi.org/10.1061/(ASCE)0733-9429(1992)118:4(615)

MELVILLE BW (1997) Pier and abutment scour: integrated approach. *J. Hydraul. Eng.* **123** (2) 125–136. https://doi.org/10.1061/(ASCE)0733-9429(1997)123:2(125)

MELVILLE BW and CHIEW YM (1999) Time scale for local scour at bridge piers. *J. Hydraul. Eng.* **125** (1) 59–65. https://doi.org/10.1061/(ASCE)0733-9429(1999)125:1(59)

MELVILLE BW and SUTHERLAND AJ (1988) Design method for local scour at bridge piers. *J. Hydraul. Eng.* **114** (10) 1210–1226. https://doi.org/10.1061/(ASCE)0733-9429(1988)114:10(1210)

MOHAMMAD V, YASER S and SHAKER HS (2016) Effects of distance between the T-shaped spur dikes on flow and scour patterns in 90 bend using the SSIIM model. *Ain Shams Eng. J.* **7** (1) 31–45. https://doi.org/10.1016/j.asej.2015.11.008

NAYYER S, FARZIN S, KARAMI H and ROSTAMI M (2019) A numerical and experimental investigation of the effects of combination of spur dikes in series on a flow field. *J. Braz. Soc. Mech. Sci. Eng.* **41** 1–11. https://doi.org/10.1007/s40430-019-1757-0

PANDEY M, AHMAD Z and SHARMA PK (2016) Estimation of maximum scour depth near a spur dike. *Can. J. Civ. Eng.* **43** (3) 270–278. https://doi.org/10.1139/cjce-2015-0280

PANDEY M, VALYRAKIS M, QI M, SHARMA A and LODHI AS (2021) Experimental assessment and prediction of temporal scour depth around a spur dike. *Int. J. Sediment Res.* **36** (1) 17–28. https://doi.org/10.1002/clen.202300135

HOSSEINI R, FAZLOULA R, SANEIE M and AMINI A (2018) Bagged neural network for estimating the scour depth around pile groups. *Int. J. River Basin Manage.* **16** (4) 401–412. https://doi.org/10.1080/15715124.2017.1372449

TRIPATHI RP and PANDEY KK (2021) Experimental study of local scour around T-shaped spur dike in a meandering channel. *Water Suppl.* **21** (2) 542–552. https://doi.org/10.2166/ws.2020.331

VAGHEFI M, RADAN P and AKBARI M (2019) Flow pattern around attractive, vertical, and repelling T-shaped spur dikes in a mild bend using CFD modeling. *Int. J. Civ. Eng.* **17** 607–617. https://doi.org/10.1007/s40999-018-0340-x

VAGHEFI M, SAFARPOOR Y and HASHEMI SS (2015) Effects of relative curvature on the scour pattern in a 90 bend with a T-shaped spur dike using a numerical method. *Int. J. River Basin Manage.* **13** (4) 501–514. https://doi.org/10.1080/15715124.2015.1049181

YANG J, ZHANG J, ZHANG Q, TENG X, CHEN W and LI X (2019) Experimental research on the maximum backwater height in front of a permeable spur dike in the bend of a spillway chute. *Water Suppl.* **19** (6) 1841–1850. https://doi.org/10.2166/ws.2019.061